J. Fluid Mech. (1994), *vol.* 266, *pp.* 121–145

Mass transport under partially reflected waves in a rectangular channel

By JIANGANG WEN AND PHILIP L.-F. LIU
School of Civil and Environmental Engineering, Cornell University, Ithaca, NY 14853, USA

(Received 10 June 1993 and in revised form 14 October 1993)

Mass transport under partially reflected waves in a rectangular channel is studied. The effects of sidewalls on the mass transport velocity pattern are the focus of this paper. The mass transport velocity is governed by a nonlinear transport equation for the second-order mean vorticity and the continuity equation of the Eulerian mean velocity. The wave slope, ka, and the Stokes boundary-layer thickness, $k(\nu/\sigma)^{\frac{1}{2}}$, are assumed to be of the same order of magnitude. Therefore convection and diffusion are equally important. For the three-dimensional problem, the generation of second-order vorticity due to stretching and rotation of a vorticity line is also included. With appropriate boundary conditions derived from the Stokes boundary layers adjacent to the free surface, the sidewalls and the bottom, the boundary value problem is solved by a vorticity-vector potential formulation; the mass transport is, in general, represented by the sum of the gradient of a scalar potential and the curl of a vector potential. In the present case, however, the scalar potential is trivial and is set equal to zero. Because the physical problem is periodic in the streamwise direction (the direction of wave propagation), a Fourier spectral method is used to solve for the vorticity, the scalar potential and the vector potential. Numerical solutions are obtained for different reflection coefficients, wave slopes, and channel cross-sectional geometry.

1. Introduction

Mass transport is a steady Lagrangian current generated by wave motions. These steady flows, although small in magnitude, are important in determining the migration of sediment near the seabed and of pollutant in the water column. Moreover, in the surf zone the vertical structure of the on–offshore mean velocity component plays an important role in transferring mean momentum flux in the longshore direction for generation of longshore currents.

The mass transport velocity pattern under a partially reflected wave train has been studied by many researchers, using various analytical, perturbation and direct numerical approaches (e.g. Longuet-Higgins 1953; Riley 1965; Haddon & Riley 1983; Iskandarani & Liu 1991). The physics for the generation of mass transport under a two-dimensional wave is fairly well understood. Because of viscous effects the mean shear stress inside the Stokes boundary layer adjacent to the solid bottom is not negligible. Consequently, a second-order (in the wave slope) mean velocity is generated inside the Stokes boundary layer and persists at the outer edge of the boundary layer. The free-surface Stokes boundary layer is weaker than the bottom boundary layer because the stress-free condition, instead of the no-slip condition, is required on the free surface. Nevertheless, a second-order mean vorticity is also induced at the outer edge of the three-surface boundary layer (Liu 1977). The residual mean vorticities at the outer edge of Stokes boundary layers are diffused into the water column in the core

region and are also advected by the mean velocity. In the very unusual situation where the wave amplitude is much smaller than the Stokes boundary-layer thickness, diffusion dominates and convection is negligible. Hence the problem is linearized and analytical conduction solutions can be obtained (Longuet-Higgins 1953). In more practical situations the wave amplitude is greater than the boundary-layer thickness. Both convection and diffusion are important and numerical solutions are usually required (Iskandarani & Liu 1991).

Many attempts have been made to verify theoretical and numerical mass transport solutions for two-dimensional waves in wave tank experiments (e.g. Russell & Osorio 1958; Mei, Liu & Carter 1972; Bijker, Kalwijk & Pieters 1974). The comparisons of the experimental and theoretical results showed a large scatter. Mei *et al.* (1972) also showed complicated three-dimensional mean circulation patterns in their wave tank study for standing waves and partially reflected waves. Among many possibilities, the effects of the sidewalls could be the major cause of the three-dimensional circulation patterns and of the discrepancies between experimental data and two-dimensional theoretical solutions. Iskandarni & Liu (1993) considered the side-wall effects for a progressive wave train. Because of the uniformity of the mass transport in the direction of wave propagation, the problem can be reduced to a two-dimensional one on the plane normal to the wave propagation direction. They solved the problem numerically using a stream function–vorticity approach and demonstrated the significant role played by the sidewalls in determining the mass transport pattern.

In most wave tank experiments the reflection from the beach (or other types of energy dissipators at one end of the tank) cannot be completely eliminated. In other experiments weakly reflected waves are intentionally generated for practical applications (Mei *et al.* 1972; Hara & Mei 1987). Therefore, a partially reflected wave train frequently exists in a wave tank. The associated mass transport velocity pattern is three-dimensional, and periodic in the direction of wave propagation. It is the objective of the present paper to develop an algorithm to examine the three-dimensional mass transport under partially reflected waves in a rectangular channel. The sidewall effects will be the focus of the investigation. Wave parameters, such as the wave slope and the reflection coefficient, and the aspect ratio of the channel will be varied.

Consider a partially reflected wave train propagating in a wave flume with a rectangular cross-section. Using the characteristic wave period, σ^{-1}, as the timescale, wavelength, k^{-1}, as the lengthscale, and the characteristic wave amplitude, a, as the scale for wave motions, the leading-order solutions, $O(\alpha) = O(ka)$, for the free-surface displacement, ζ, and the irrotational velocity components, (u_1, v_1, w_1), which are of $O(\sigma a)$, can be expressed in the following dimensionless forms:

$$\zeta = (\mathrm{e}^{\mathrm{i}x} + R\mathrm{e}^{-\mathrm{i}x})\,\mathrm{e}^{-\mathrm{i}t}, \tag{1}$$

$$\boldsymbol{v}_1 = \begin{Bmatrix} u_1 \\ v_1 \\ w_1 \end{Bmatrix} = \begin{Bmatrix} U \\ V \\ W \end{Bmatrix} \mathrm{e}^{-\mathrm{i}t}. \tag{2}$$

$$\left.\begin{aligned} U &= \frac{\cosh(z+h)}{\sinh h}(\mathrm{e}^{\mathrm{i}x} - R\mathrm{e}^{-\mathrm{i}x}), \\ V &= 0, \\ W &= -\frac{\mathrm{i}\sinh(z+h)}{\sinh h}(\mathrm{e}^{\mathrm{i}x} + R\mathrm{e}^{-\mathrm{i}x}), \end{aligned}\right\} \tag{3}$$

in which R denotes a complex reflection coefficient, $0 \leqslant |R| \leqslant 1$. The partially reflected

wave train propagates forwards and backwards in the x-direction. The no-flux boundary conditions on the bottom of the channel, $z = -h$, and on the sidewalls, $y = 0, b$, are satisfied by the first-order potential flow field.

To satisfy the no-slip condition along the sidewalls and the bottom of the tank and the no-stress condition on the free surface, Stokes boundary layers exist adjacent to the boundaries. The boundary-layer solutions are well known and will not be repeated here (e.g. see Mei & Liu 1973).

In the following sections, we will first discuss the governing equations and boundary conditions for the mass transport velocity in a rectangular channel. A vorticity-vector potential formulation is introduced by representing the mass transport velocity as the sum of the gradient of a scalar potential and the curl of a vector potential. Because of the periodicity of the mass transport velocity in the direction of wave propagation, a Fourier spectral method is used to solve for the harmonic components of mean vorticity, vector potential and the mass transport velocity. The scalar potential is a trivial solution for the wave channel case and is set to be zero. Numerical solutions are obtained for different wave parameters, i.e. wave slopes and reflection coefficients, and geometrical parameters, i.e. the depth-to-width ratio of the rectangular channel. Numerical results are compared to existing theoretical and experimental data for special cases.

2. Governing equations for mass transport

The governing equations for the second-order $O(\alpha^2)$, mass transport velocity, $\boldsymbol{v}_m$, can be written in terms of the transport equation for the second-order steady vorticity (Dore 1976):

$$\delta^2 \nabla^2 \boldsymbol{\omega} + \nabla \times (\boldsymbol{v}_m \times \boldsymbol{\omega}) = 0. \tag{4}$$

Because the mass transport is a Lagrangian quantity, the Eulerian streaming velocity $\boldsymbol{v}$ is related to $\boldsymbol{v}_m$ through (Longuet-Higgins 1953)

$$\boldsymbol{v} = \boldsymbol{v}_m - \boldsymbol{v}_s, \tag{5}$$

in which $\boldsymbol{v}_s$, the Stokes drift, represents the cumulative drift velocity experienced by a fluid particle moving through a non-uniform flow field. The steady vorticity $\boldsymbol{\omega}$ is also an Eulerian quantity and is defined in terms of the streaming velocity

$$\boldsymbol{\omega} = \nabla \times \boldsymbol{v}, \tag{6}$$

and the latter satisfies the continuity equation

$$\nabla \cdot \boldsymbol{v} = 0. \tag{7}$$

In the vorticity transport equation (4), the parameter δ describes the ratio of the thickness of the Stokes boundary layer to the wave amplitude, i.e.

$$\delta = \frac{1}{a}\left(\frac{\nu}{\sigma}\right)^{\frac{1}{2}} = \frac{1}{ka}\left(\frac{k^2\nu}{\sigma}\right)^{\frac{1}{2}} = \frac{\epsilon}{\alpha}. \tag{8}$$

Diffusion dominates when δ^2 is larger; the governing equation can then be linearized by discarding the nonlinear terms. On the other hand, when δ^2 is small the balance between diffusion and convection can be achieved within a small region, $O(\delta)$, in the vicinity of the Stokes layers. In a typical laboratory set-up, the parameter δ is of $O(10^{-1})$. Hence the full nonlinear equation (4) will be solved in conjunction with (6), (7) and appropriate boundary conditions.

The Stokes drift $\boldsymbol{v}_s$ can be expressed in terms of the first-order velocity field as follows:

$$\boldsymbol{v}_s = \overline{\int_{t_0}^{t} \boldsymbol{v}_1 \, \mathrm{d}t' \cdot \nabla \boldsymbol{v}_1}, \tag{9}$$

in which the overbar denotes the time average over a characteristic wave period. For the partially reflected wave train, given in (2) and (3), the Stokes drift can be calculated as

$$\boldsymbol{v}_s = (u_s, v_s, w_s) = \left(\frac{\cosh 2(z+h)}{2 \sinh^2 h} (1 - RR^*), 0, 0 \right), \tag{10}$$

where the asterisk indicates the complex conjugate. The Stokes drift is unidirectional and divergence free.

3. Boundary conditions for mass transport

To obtain solutions for the Eulerian streaming and the associated steady vorticity in the core region, boundary conditions must be specified along the outer edge of the Stokes layers adjacent to the free surface, the sidewalls and the bottom. These conditions can be readily obtained from the existing theories (e.g. Mei 1989; Liu 1977).

3.1. *Boundary conditions on the free surface* ($z = 0$)

Liu (1977) studied the three-dimensional free-surface boundary layer and showed that the horizontal components of the wave-induced steady vorticity at the outer edge of the Stokes layer are

$$\left.\begin{aligned} \omega^x &= \mathrm{Im}\left[\frac{\partial W}{\partial x}\frac{\partial V^*}{\partial x} + \frac{\partial W}{\partial y}\frac{\partial V^*}{\partial y} + \frac{\partial W}{\partial z}\frac{\partial V^*}{\partial z} \right]_{z=0}, \\ \omega^y &= \mathrm{Im}\left[\frac{\partial W}{\partial x}\frac{\partial U^*}{\partial x} + \frac{\partial W}{\partial y}\frac{\partial U^*}{\partial y} + \frac{\partial W}{\partial z}\frac{\partial U^*}{\partial z} \right]_{z=0}, \end{aligned}\right\} \tag{11}$$

where Im denotes the imaginary part. Using the leading-order velocity in (3), we find the boundary conditions for the mean vorticity components on the free surface:

$$\omega^x = 0, \quad \omega^y = \frac{\sinh 2h}{\sinh^2 h}(1 - RR^*) \quad \text{on} \quad z = 0. \tag{12}$$

Note that both vorticity components vanish for a standing wave, i.e. $R = 1$. For the steady flow the mean free surface ($z = 0$) is a material surface; therefore the vertical mean velocity vanishes

$$w = 0 \quad \text{on} \quad z = 0. \tag{13}$$

3.2. *Boundary conditions on the central plane* ($y = \frac{1}{2}b$)

In the rectangular channel the mass transport velocity is symmetric with respect to the central plane, $y = \frac{1}{2}b$. Because of the symmetry only one half of the channel is considered, $0 \leqslant y \leqslant \frac{1}{2}b$. The following conditions for the second-order streaming velocity must be true on the central plane:

$$\frac{\partial u}{\partial y} = 0, \quad v = 0, \quad \frac{\partial w}{\partial y} = 0 \quad \text{on} \quad y = \tfrac{1}{2}b. \tag{14}$$

Consequently, the steady vorticity must satisfy the following boundary conditions:

$$\omega^x = \frac{\partial w}{\partial y} - \frac{\partial v}{\partial z} = 0 \quad \omega^z = \frac{\partial v}{\partial x} - \frac{\partial u}{\partial y} = 0, \quad \frac{\partial \omega^y}{\partial y} = 0 \quad \text{on} \quad y = \tfrac{1}{2}b. \tag{15}$$

3.3. *Boundary conditions on the bottom* ($z = -h$)

Mei (1989) presented formulae for the steady streaming at the outer edge of the Stokes layer near the bottom:

$$\left.\begin{aligned} u &= -\tfrac{1}{4}\mathrm{Re}\left[3(1-\mathrm{i})\,U\frac{\partial U^*}{\partial x} + V\frac{\partial U^*}{\partial y} + (2-3\mathrm{i})\,U\frac{\partial V^*}{\partial y}\right]_{z=-h}, \\ v &= -\tfrac{1}{4}\mathrm{Re}\left[3(1-i)\,V\frac{\partial V^*}{\partial y} + U\frac{\partial V^*}{\partial x} + (2-3\mathrm{i})\,V\frac{\partial U^*}{\partial x}\right]_{z=-h}, \\ w &= 0, \end{aligned}\right\} \tag{16}$$

in which Re denotes the real part. For the partially reflected wave train the streaming velocity can be specifically written as

$$\left.\begin{aligned} u &= \frac{3}{4\sinh^2 h}[-\mathrm{i}R\,\mathrm{e}^{-\mathrm{i}2x} + (1-RR^*) + \mathrm{i}R^*\,\mathrm{e}^{\mathrm{i}2x}] \\ v &= w = 0 \end{aligned}\right\} \quad \text{on} \quad z = -h. \tag{17}$$

For the progressive wave case ($R = 0$) the streaming velocity is in the direction of wave propagation. On the other hand, under a standing wave ($R = 1$), the streaming velocity diverges from the nodal points ($x = (n+\frac{1}{2})\pi$, $n = 0, 1, 2, \ldots$) and converges at the anti-nodal points ($x = n\pi$, $n = 0, 1, 2, \ldots$).

3.4. *Boundary conditions at the sidewall* ($y = 0$)

The sidewall is located at $y = 0$. Along the outer edge of the Stokes layer the Eulerian streaming can be obtained by substituting W and z for V and y in (16), respectively. Using (3) in the resulting formulae, we obtain

$$\left.\begin{aligned} u &= \frac{1}{4\sinh^2 h}[-\mathrm{i}R\,\mathrm{e}^{-\mathrm{i}2x} + \mathrm{i}R^*\,\mathrm{e}^{\mathrm{i}2x}] \\ v &= 0 \\ w &= -\frac{\sinh 2(z+h)}{4\sinh^2 h}(1+RR^*) \end{aligned}\right\} \quad \text{on} \quad y = 0. \tag{18}$$

Note that a negative (downwards) vertical velocity exists independent of the reflection coefficient. In the streamwise direction the streaming vanishes for progressive waves. For a standing wave the steady streaming moves from the nodal points to the anti-nodal points, which is the same as the flow direction outside of the bottom Stokes layer.

4. Vorticity-vector potential formulation for mass transport

For the channel problem, the Stokes drift (10) is divergence free, i.e. $\nabla\cdot\boldsymbol{v}_s = 0$. Therefore from (5) and (7) the mass transport velocity $\boldsymbol{v}_m$ is also a solenoidal vector,

$$\nabla\cdot\boldsymbol{v}_m = 0. \tag{19}$$

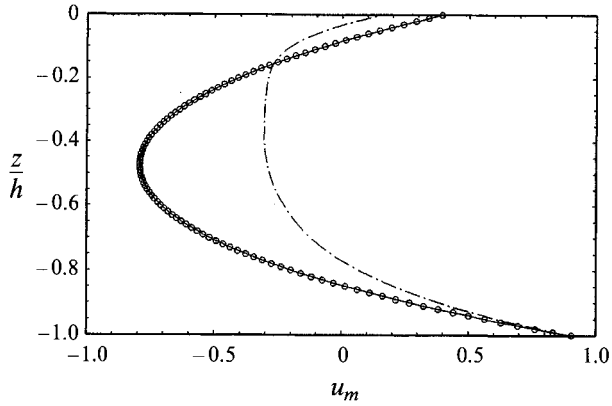

FIGURE 1. Comparisons between analytical and numerical solutions for the streamwise mass transport velocity u_m on the central plane ($y/b = 0.5$) for large δ: ——, analytical solutions for infinite δ; ooo, numerical solutions for $\delta = 5 \times 10^5$; – – –, numerical solutions for $\delta = 0.1$. The cross-section of the channel is a square ($b/h = 1$, $h = 1$).

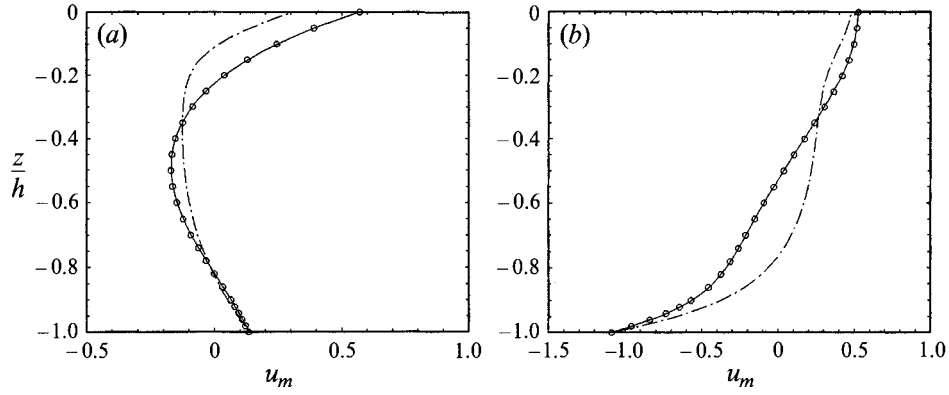

FIGURE 2. Verification of the present numerical scheme with known two-dimensional numerical solutions for u_m at $x = \frac{1}{4}\pi$, $y/b = 0.5$, with $\delta = 0.1$: ooo, two-dimensional solutions (Iskandarani & Liu 1991); ——, two-dimensional solutions of the present scheme without the sidewall effects; – – –, three-dimensional numerical solutions of the present scheme including the sidewall effects: (*a*) $R = 0.5$, (*b*) $R = 1.0$.

Thus $\boldsymbol{v}_m$ can be expressed in terms of a scalar potential ϕ and a vector potential $\boldsymbol{\psi}$ (Hirasaki & Hellums 1968, 1970):

$$\boldsymbol{v}_m = \boldsymbol{\nabla}\phi + \boldsymbol{\nabla} \times \boldsymbol{\psi}, \tag{20}$$

with

$$\nabla^2\phi = 0. \tag{21}$$

Hirasaki & Hellums (1970) have also demonstrated that a unique solenoidal vector potential $\boldsymbol{\psi}$ exists. Upon taking the curl of (20), one obtains a Poisson equation for $\boldsymbol{\psi}$:

$$\boldsymbol{\omega}_m = \boldsymbol{\omega} + \boldsymbol{\omega}_s = -\nabla^2\boldsymbol{\psi}, \tag{22}$$

in which the steady streaming vorticity associated with the Stokes drift can be calculated from (10):

$$\boldsymbol{\omega}_s = (\omega_s^x, \omega_s^y, \omega_s^z) = \left(0, \frac{\sinh 2(z+h)}{\sinh^2 h}(1 - RR^*), 0\right), \tag{23}$$

and only the spanwise component is non-zero.

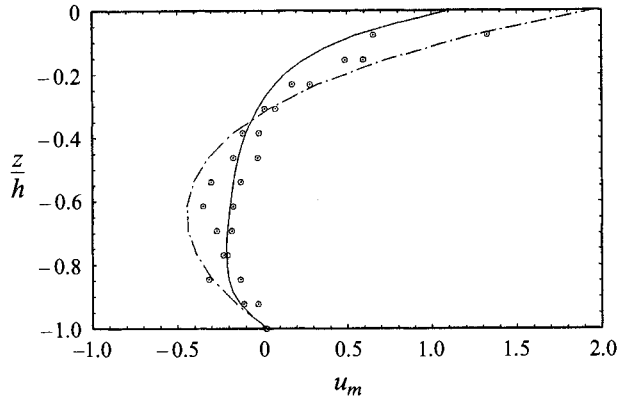

FIGURE 3. Comparison between experimental data and theoretical solutions for u_m; $kh = 2.56$, $b = 76$ cm, $h = 13$ cm, $\delta = 0.059$: —·—, Longuet-Higgins' two-dimensional solutions (1953); ⊙ ⊙ ⊙, experimental data (Mei *et al.* 1972) on the central plane; ——, present results on the central plane.

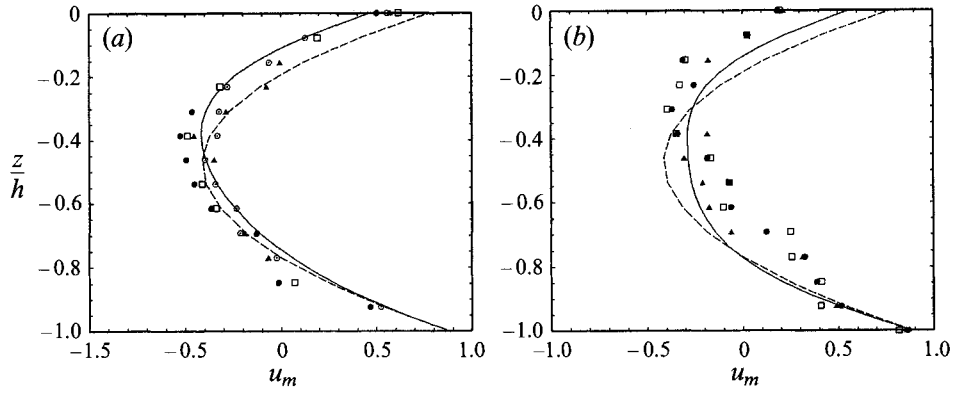

FIGURE 4. Comparison between experimental data and theoretical solutions for u_m; $kh = 1.02$, $\delta = 0.034$: symbols are experimental data (Mei *et al.* 1972); ——, Longuet-Higgins' two-dimensional solutions (1953); ——, present results: (*a*) 5 cm from the sidewall; (*b*) the central plane.

Instead of solving (4), (6) and (7) for ω and $\boldsymbol{v}$, we plan to solve (4), (21) and (22) for ω, ϕ and ψ. From the boundary conditions presented in the previous section the mass transport associated with a partially reflected wave train must be periodic in the streamwise direction (the x-direction). Hence the dependent variables can be expressed in a Fourier expansion:

$$\begin{Bmatrix} \phi \\ \psi \\ \boldsymbol{v}_m \\ \omega \end{Bmatrix} = \sum_{n=-N}^{N} e^{2inx} \begin{Bmatrix} \varphi_n(y,z) \\ \boldsymbol{\Psi}_n(y,z) \\ \boldsymbol{v}_{m,n}(y,z) \\ \boldsymbol{\Omega}_n(y,z) \end{Bmatrix} \tag{24}$$

Substituting the Fourier expansion for ϕ into the Laplace equation (21), we obtain

$$\frac{\partial^2 \varphi_n}{\partial y^2} + \frac{\partial^2 \varphi_n}{\partial z^2} - 4n^2 \varphi_n = 0, \quad n = 0, \pm 1, \pm 2, \ldots, \pm N. \tag{25}$$

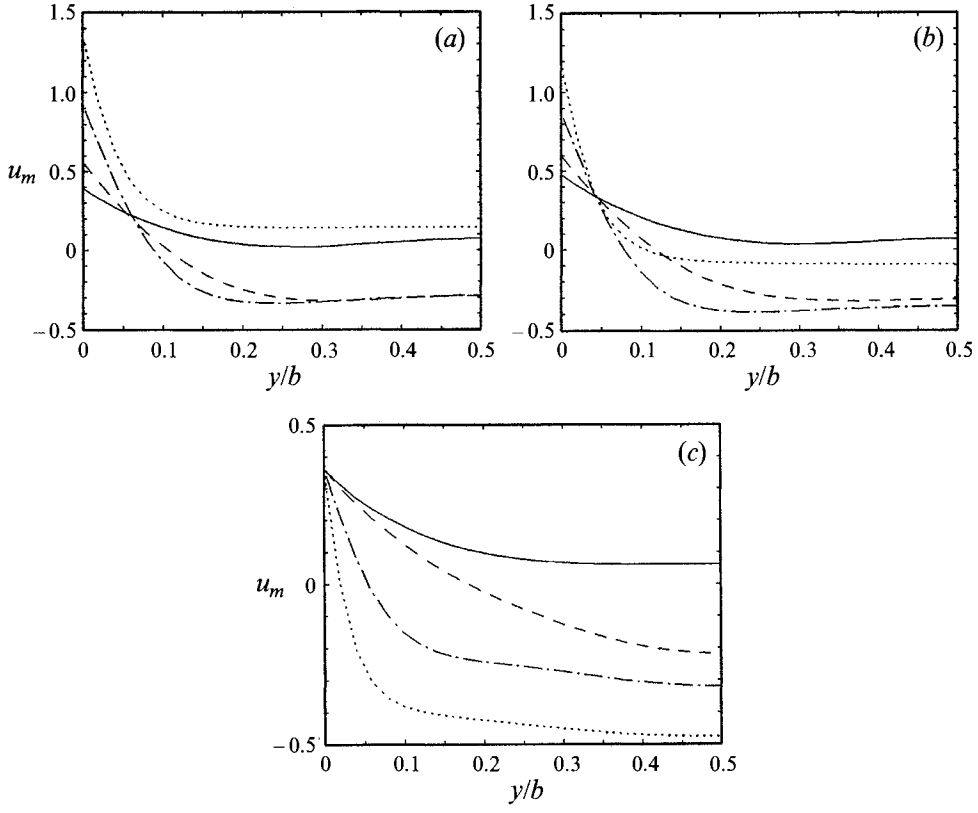

FIGURE 5. Spanwise profiles of u_m at several different elevations on the plane $x = -\frac{1}{4}\pi$, in a rectangular channel with a square cross-section: ——, $z/h = -0.8$; — —, $z/h = -0.5$; — · —, $z/h = -0.2$; - - - - -, $z/h = 0$: (*a*) $R = 0$; (*b*) $R = 0.5$; (*c*) $R = 1.0$.

The boundary conditions derived in the previous section show that the normal mass transport velocity component vanishes along the entire boundary: the free surface, the sidewall, the bottom and the central plane. This implies that from (20)

$$\boldsymbol{n}\cdot\boldsymbol{v}_m = \boldsymbol{n}\cdot\nabla\phi + \boldsymbol{n}\cdot\nabla\times\boldsymbol{\psi} = 0, \tag{26}$$

where $\boldsymbol{n}$ denotes the unit normal along the boundaries. We require that

$$\boldsymbol{n}\cdot\nabla\phi = 0 \tag{27}$$

along the boundaries and the components of $\boldsymbol{\psi}$ tangential to the boundaries be zero along these boundaries. From the solenoidal condition for $\boldsymbol{\psi}$, $\nabla\cdot\boldsymbol{\psi} = 0$, the normal derivative of the normal component of the vector potential must vanish along the boundaries such that (26) is satisfied. Specifically, these conditions can be expressed as

$$\Psi_n^x = \Psi_n^y = \frac{\partial \Psi_n^z}{\partial z} = 0 \quad \text{on} \quad z = 0, -h, \tag{28}$$

along the free surface and the bottom, and

$$\Psi_n^x = \Psi_n^z = \frac{\partial \Psi_n^y}{\partial y} = 0 \quad \text{on} \quad y = 0, \tfrac{1}{2}b, \tag{29}$$

along the sidewall and the central plane.

The governing equation (25) and the boundary condition (27) are homogeneous. Hence the scalar potential ϕ for the present problem is trivial (i.e. $\varphi_n = 0$, for $n \neq 0$,

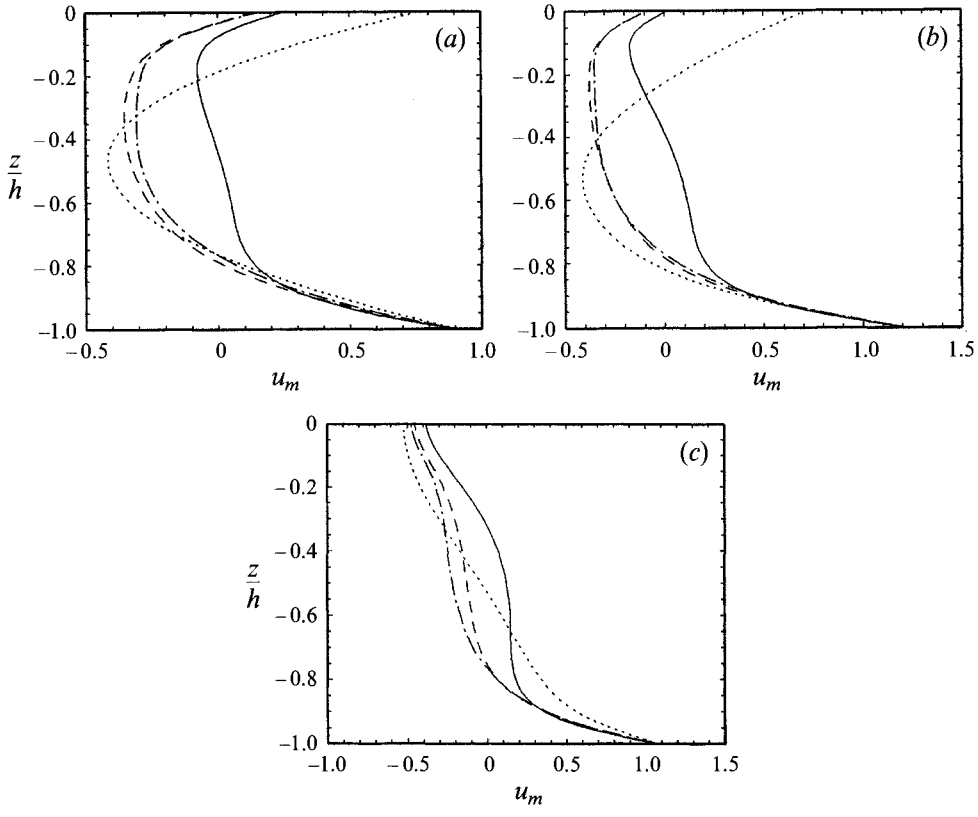

FIGURE 6. Vertical profiles of u_m at several different distances from the sidewall on the plane $x = -\frac{1}{4}\pi$: ——, $y/b = 0.1$; – – –, $y/b = 0.3$; —·—, $y/b = 0.5$; - - - - -, the two-dimensional solutions: (*a*) $R = 0$; (*b*) $R = 0.5$; (*c*) $R = 1.0$

and φ_0 = an arbitrary constant). Our problem can be simplified significantly and the mass transport velocity can be written in term of the vector potential only:

$$\boldsymbol{v}_m = \nabla \times \boldsymbol{\Psi}. \tag{30}$$

When expressed in terms of the Fourier components of the vector potential and the vorticity, the Poisson equation (22) becomes

$$\frac{\partial^2 \boldsymbol{\Psi}_n}{\partial y^2} + \frac{\partial^2 \boldsymbol{\Psi}_n}{\partial z^2} - 4n^2 \boldsymbol{\Psi}_n = -\boldsymbol{\Omega}_n - \boldsymbol{\Omega}_{s,n}, \quad n = 0, \pm 1, \pm 2, \ldots, \pm N, \tag{31}$$

where the subscript s represents the vorticity associated with the Stokes drift. The boundary conditions for $\boldsymbol{\Psi}_n$ are given in (28) and (29).

Substituting the Fourier components (24) into the transport equation for the steady vorticity, (4), we obtain

$$\frac{\partial^2 \boldsymbol{\Omega}_n}{\partial y^2} + \frac{\partial^2 \boldsymbol{\Omega}_n}{\partial z^2} - 4n^2 \boldsymbol{\Omega}_n + \boldsymbol{f}_n = 0, \quad n = 0, \pm 1, \pm 2, \ldots, \pm N, \tag{32}$$

where $\boldsymbol{f}_n$ are the Fourier coefficients of the nonlinear convection and vortex stretching term, i.e.

$$\sum_{n=-N}^{N} \boldsymbol{f}_n e^{2inx} = \nabla \times (\boldsymbol{v}_m \times \boldsymbol{\omega}) = \boldsymbol{\omega} \cdot \nabla \boldsymbol{v}_m - \boldsymbol{v}_m \cdot \nabla \boldsymbol{\omega}. \tag{33}$$

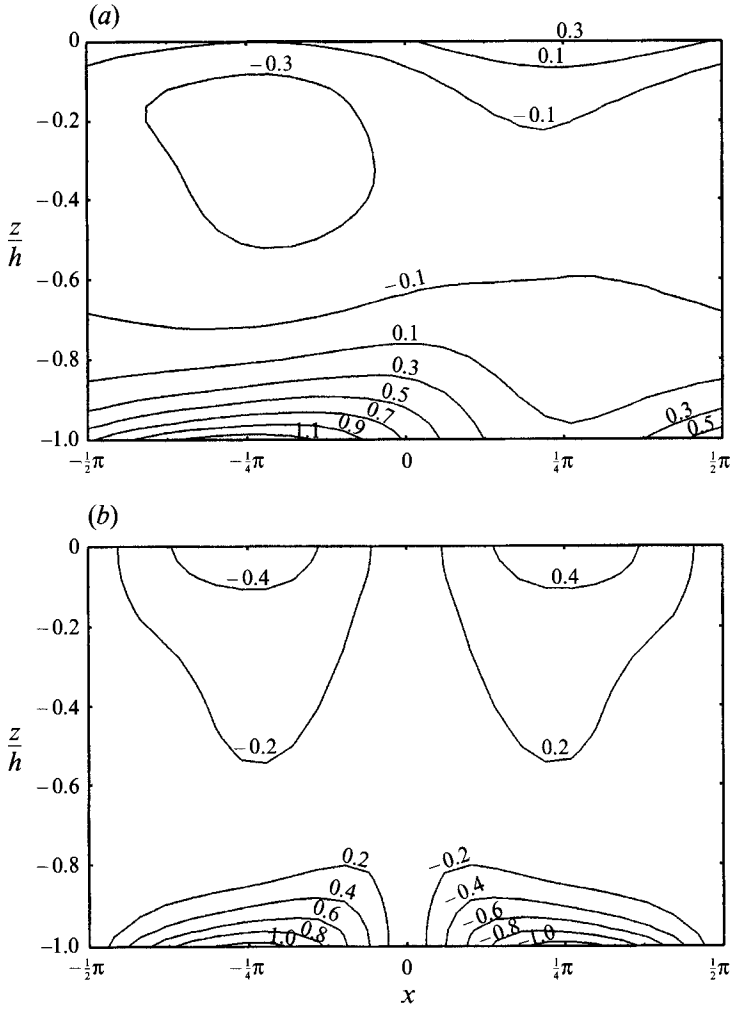

FIGURE 7. Contour lines of u_m on the central plane ($y/b = 0.5$): (*a*) $R = 0.5$; (*b*) $R = 1.0$.

The boundary conditions of the Fourier components of the vorticity, $\boldsymbol{\Omega}_n$, can be obtained by substituting (24) into the boundary conditions derived from the previous section. For instance from (12) the boundary conditions on the free surface can be written as

$$\Omega_n^x = 0 \quad \text{on} \quad z = 0, \tag{34}$$

$$\left.\begin{aligned} \Omega_0^y &= \frac{\sinh 2h}{\sinh^2 h}(1 - RR^*) \\ \Omega_n^y &= 0 \quad \text{for} \quad n \neq 0 \end{aligned}\right\} \quad \text{on} \quad z = 0. \tag{35}$$

Since the vorticity is solenoidal, the boundary condition for the vertical component of the vorticity becomes

$$\frac{\partial \Omega_n^z}{\partial z} = 0 \quad \text{on} \quad z = 0. \tag{36}$$

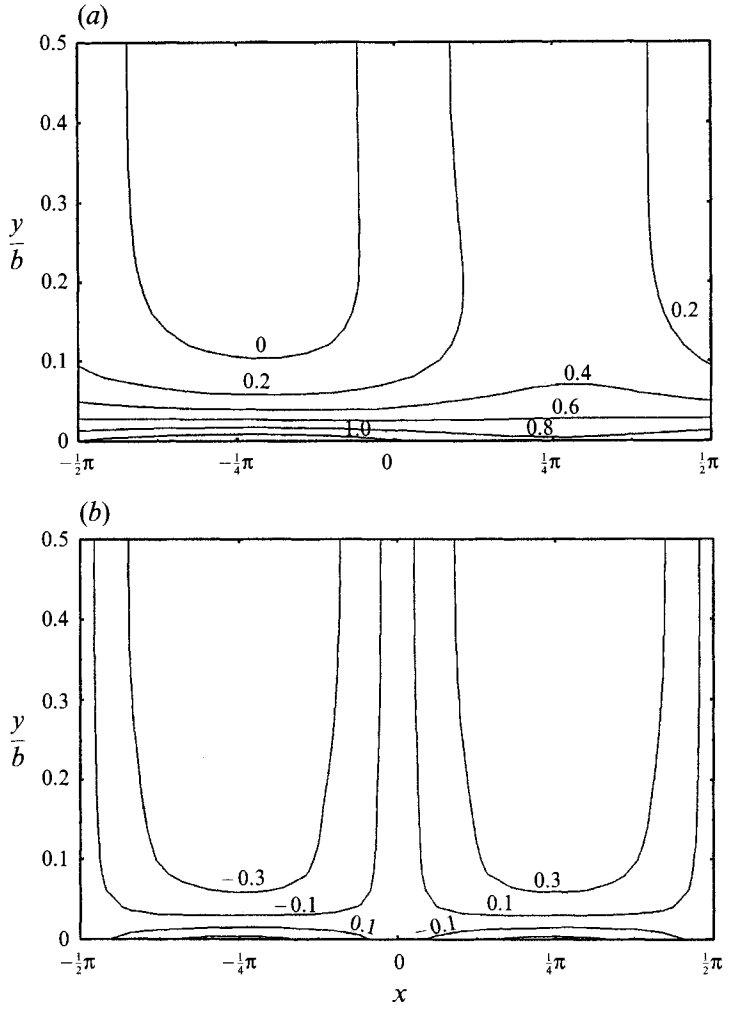

FIGURE 8. Contour lines of u_m on the free surface ($z/h = 0$): (*a*) $R = 0.5$; (*b*) $R = 1.0$.

Similarly, the boundary conditions along the central plane, (15), can be converted into a Fourier component form:

$$\Omega_n^x = 0 \quad \Omega_n^z = 0, \quad \frac{\partial \Omega_n^y}{\partial y} = 0 \quad \text{on} \quad y = \tfrac{1}{2}b. \tag{37}$$

At the bottom ($z = -h$) the vorticity components can be written as

$$\Omega_n^x = -\frac{\partial v_n}{\partial z}, \quad \Omega_n^y = -\frac{\partial u_n}{\partial z}, \quad \Omega_n^z = 0 \quad \text{on} \quad z = -h. \tag{38}$$

Note that u_n and v_n are specified along the bottom, (17). The normal derivatives of these velocity components are not known. A second-order finite-difference approximation will be employed to calculate these boundary conditions.

Along the sidewall boundary, a similar situation exists. The vorticity components are written as

$$\Omega_n^x = \frac{\partial w_n}{\partial y}, \quad \Omega_n^y = 0, \quad \Omega_n^z = -\frac{\partial u_n}{\partial y} \quad \text{on} \quad y = 0, \tag{39}$$

in which u_n and v_n are given in (18).

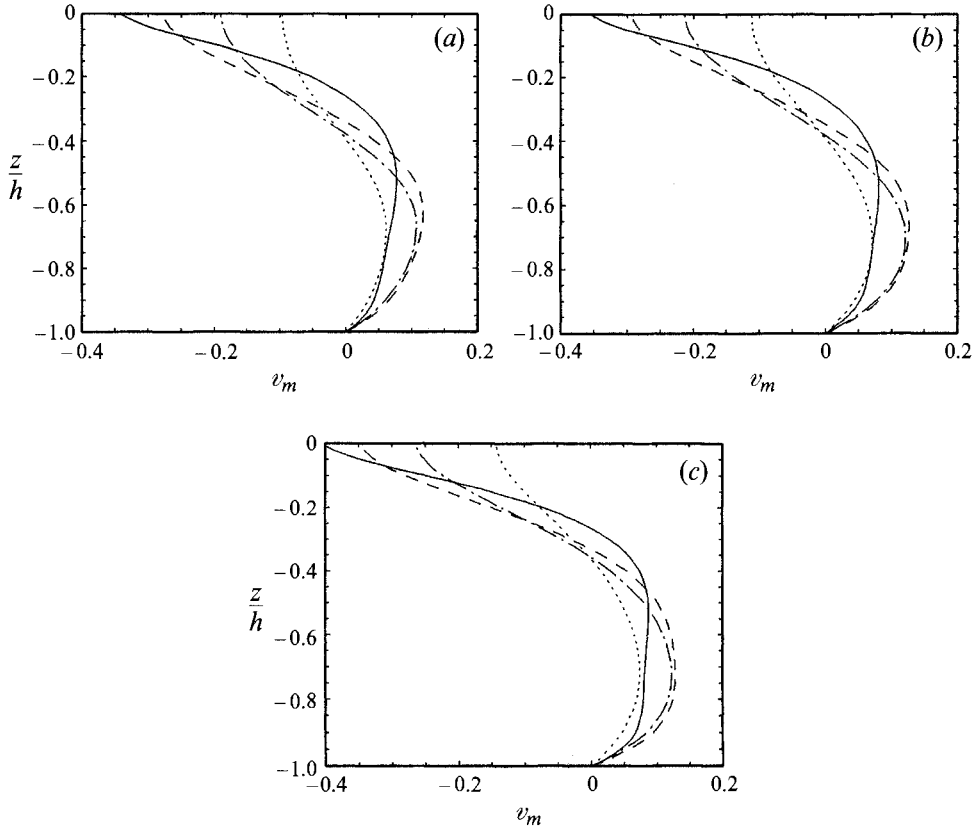

FIGURE 9. Vertical profiles of v_m at several different distances from the sidewall on the plane $x = -\frac{1}{4}\pi$: ——, $y/b = 0.1$; – – –, $y/b = 0.2$; —·—, $y/b = 0.3$; - - - - -, $y/b = 0.5$: (*a*) $R = 0$; (*b*) $R = 0.5$; (*c*) $R = 1.0$.

We remark here that the zero-net-flux condition across the vertical cross-section of the channel is naturally satisfied in the vorticity-vector potential approach. From (30) and (24) the streamwise mass transport velocity can be written as

$$u_m = \frac{\partial \psi^z}{\partial y} - \frac{\partial \psi^y}{\partial z} = \sum_{n=-N}^{N} \left(\frac{\partial \Psi_n^z}{\partial y} - \frac{\partial \Psi_n^y}{\partial z} \right) e^{2inx}. \tag{40}$$

The net mass transport flux across a vertical plane normal to the direction of wave propagation is

$$q_m = \int_0^{\frac{1}{2}b} \int_{-h}^{0} u_m \, dy \, dz = \sum_{n=-N}^{N} \int_0^{\frac{1}{2}b} \int_{-h}^{0} \left(\frac{\partial \Psi_n^z}{\partial y} - \frac{\partial \Psi_n^y}{\partial z} \right) e^{2inx} \, dy \, dz. \tag{41}$$

Integrating the above equation and employing boundary conditions (28) and (29), we can show that the net mass transport flux is zero, i.e.

$$q_m = \sum_{n=-N}^{N} e^{2inx} \left[\int_{-h}^{0} (\Psi_n^z|_{y=\frac{1}{2}b} - \Psi_n^z|_{y=0}) \, dz - \int_0^{\frac{1}{2}b} (\Psi_n^y|_{z=0} - \Psi_n^y|_{z=-h}) \, dy \right] = 0. \tag{42}$$

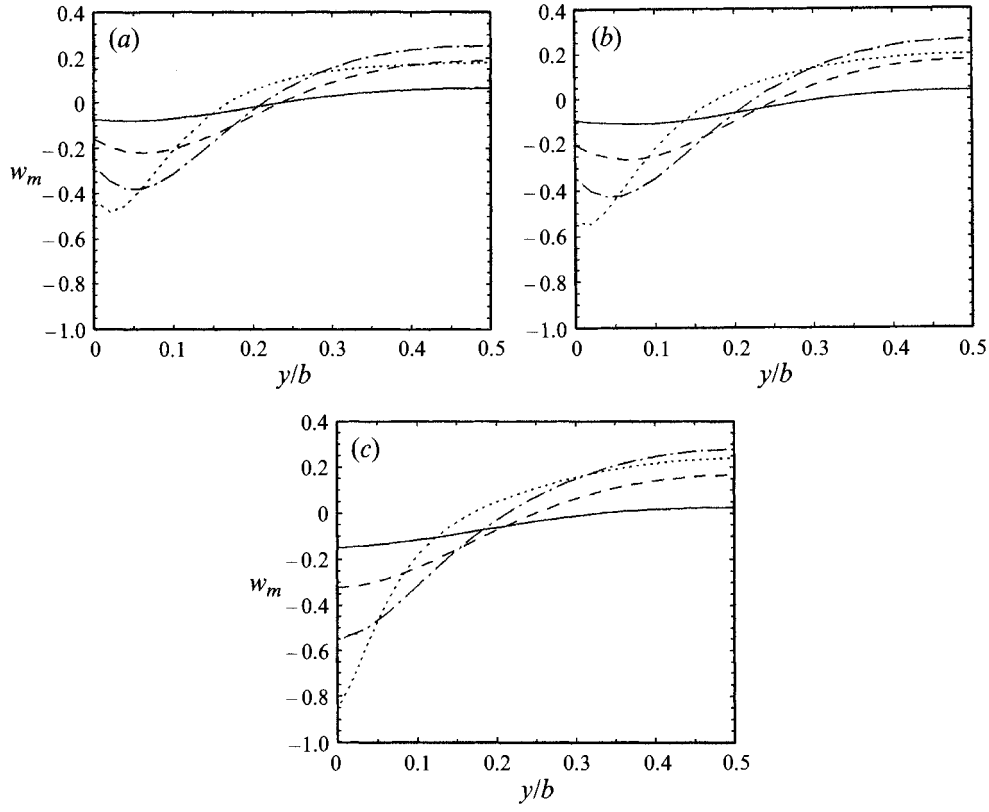

FIGURE 10. Spanwise profiles of w_m at several different elevations on the plane $x = -\frac{1}{4}\pi$: ——, $z/h = -0.8$; — —, $z/h = -0.6$; —·—, $z/h = -0.4$; -----, $z/h = -0.2$; (*a*) $R = 0$; (*b*) $R = 0.5$; (*c*) $R = 1.0$.

5. Numerical scheme

The vorticity equation (32) is nonlinear. To solve it numerically, a fictitious time derivative term is introduced into the equation, i.e.

$$\frac{\partial \boldsymbol{\Omega}_n}{\partial t} = \frac{\partial^2 \boldsymbol{\Omega}_n}{\partial y^2} + \frac{\partial^2 \boldsymbol{\Omega}_n}{\partial z^2} - 4n^2 \boldsymbol{\Omega}_n + \boldsymbol{f}. \tag{43}$$

Therefore, the true solution is the steady-state limit of the above equation. Approximating (43) with a forward finite difference in time, we get

$$\mathrm{D}^2 \boldsymbol{\Omega}_n^{k+1} - \left(4n^2 + \frac{1}{\Delta t}\right) \boldsymbol{\Omega}_n^{k+1} = -\left(\boldsymbol{f}_n^k + \frac{\boldsymbol{\Omega}_n^k}{\Delta t}\right), \quad n = 0, \pm 1, \pm 2, \ldots, \pm N, \tag{44}$$

where

$$\mathrm{D}^2 = \frac{\partial^2}{\partial y^2} + \frac{\partial^2}{\partial z^2},$$

and Δt is the time step. The superscripts, k and $k+1$, represent the time level. By using the implicit finite-difference scheme, (44), the original equation (43) has been linearized at the previous time level. Specifically, the nonlinear term can be expressed as

$$\boldsymbol{f}_n^k = \sum_{l=-N}^{N} \begin{pmatrix} \boldsymbol{\Omega}_l \cdot \mathrm{L}_{n-l} u_{m,n-l} - \boldsymbol{v}_{m,l} \cdot \mathrm{L}_{n-l} \Omega_{n-l}^x \\ \boldsymbol{\Omega}_l \cdot \mathrm{L}_{n-l} v_{m,n-l} - \boldsymbol{v}_{m,l} \cdot \mathrm{L}_{n-l} \Omega_{n-l}^y \\ \boldsymbol{\Omega}_l \cdot \mathrm{L}_{n-l} w_{m,n-l} - \boldsymbol{v}_{m,l} \cdot \mathrm{L}_{n-l} \Omega_{n-l}^z \end{pmatrix}^k, \tag{45}$$

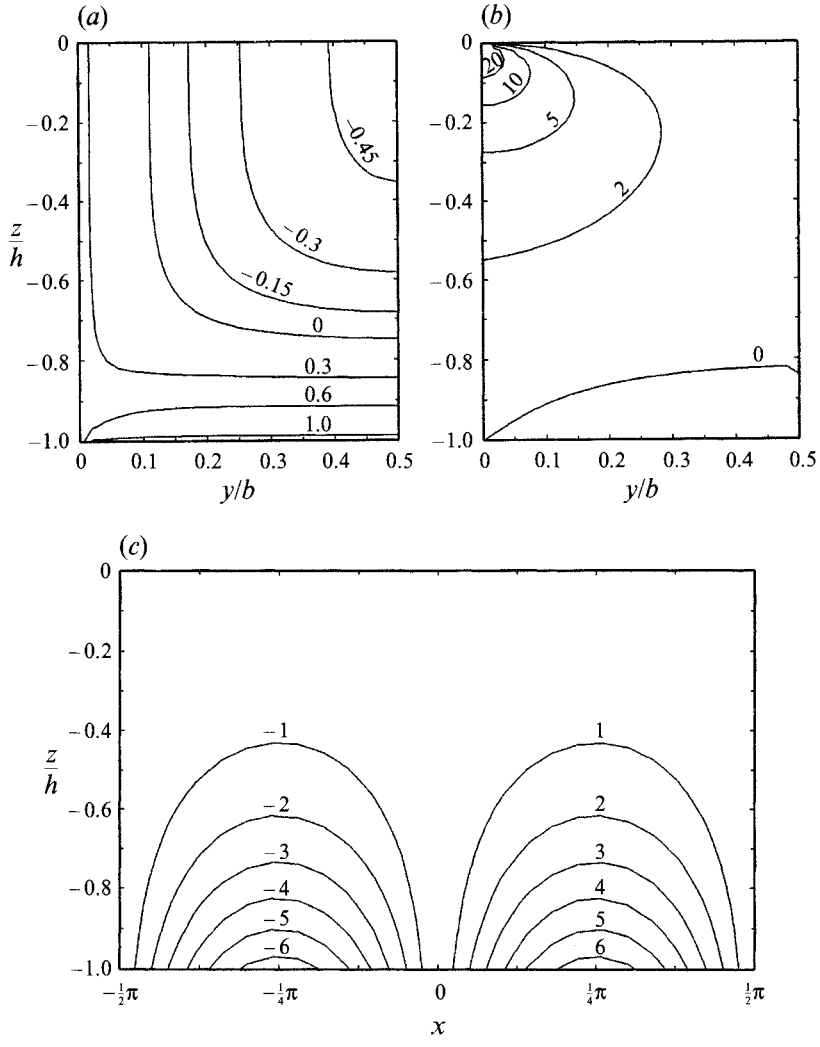

FIGURE 11. Contour lines of u_m, ω^x and ω^y under a standing wave for $\delta = 100$: (*a*) streamwise mass transport velocity u_m at $x = -\frac{1}{4}\pi$; (*b*) streamwise vorticity ω^x at $x = -\frac{1}{4}\pi$; (*c*) spanwise vorticity ω^y on the central plane ($y/b = 0.5$).

where $$\mathrm{L}_{n-l} = \left(2(n-l)\,\mathrm{i}, \frac{\partial}{\partial y}, \frac{\partial}{\partial z}\right).$$

To calculate the mass transport velocity we must solve the vector potential first. The governing equation for the vector potential, (31), can be written as

$$\mathrm{D}^2 \boldsymbol{\Psi}_n^k - 4n^2 \boldsymbol{\Psi}_n^k = -\boldsymbol{\Omega}_n^k - \boldsymbol{\Omega}_{s,n}^k. \tag{46}$$

Once $\boldsymbol{\Psi}_n^k$ is found, the mass transport velocity can be calculated from the definition, (30), i.e.

$$\boldsymbol{v}_m^k = \nabla \times \boldsymbol{\psi}^k = \sum_{n=-N}^{N} \mathrm{e}^{2\mathrm{i}nx} \begin{pmatrix} u_m \\ v_m \\ w_m \end{pmatrix}_n^k, \tag{47}$$

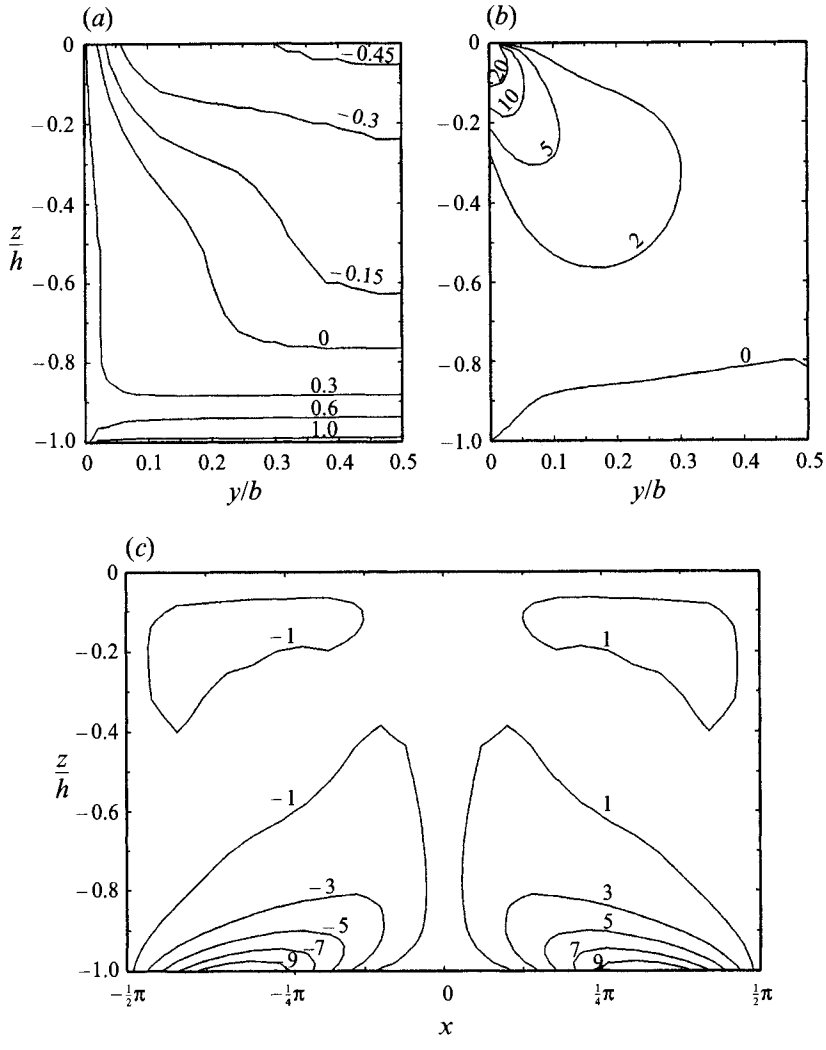

FIGURE 12. As figure 11 but for $\delta = 0.1$.

$$\left.\begin{aligned} u_m^k &= \sum_{n=-N}^{N} \mathrm{e}^{2\mathrm{i}nx}\left(\frac{\partial \Psi^z}{\partial y} - \frac{\partial \Psi^y}{\partial z}\right)^k, \\ v_m^k &= \sum_{n=-N}^{N} \mathrm{e}^{2\mathrm{i}nx}\left(\frac{\partial \Psi^x}{\partial z} - 2\mathrm{i}n\Psi^z\right)^k, \\ w_m^k &= \sum_{n=-N}^{N} \mathrm{e}^{2\mathrm{i}nx}\left(2\mathrm{i}n\Psi^y - \frac{\partial \Psi^x}{\partial y}\right)^k. \end{aligned}\right\} \tag{48}$$

The vorticity equation (44) and the vector potential equation (46) consist of six sets of Helmholtz equations. The spatial derivatives in those equations are approximated by the second-order central-finite-difference formulae. The resulting system of algebraic equations is solved by fast Fourier transforms.

The numerical procedure can be summarized as follows:

(i) Given the vorticity at the kth time level, the vector potential at the same time level is obtained by solving (46) with boundary conditions (28) and (29).

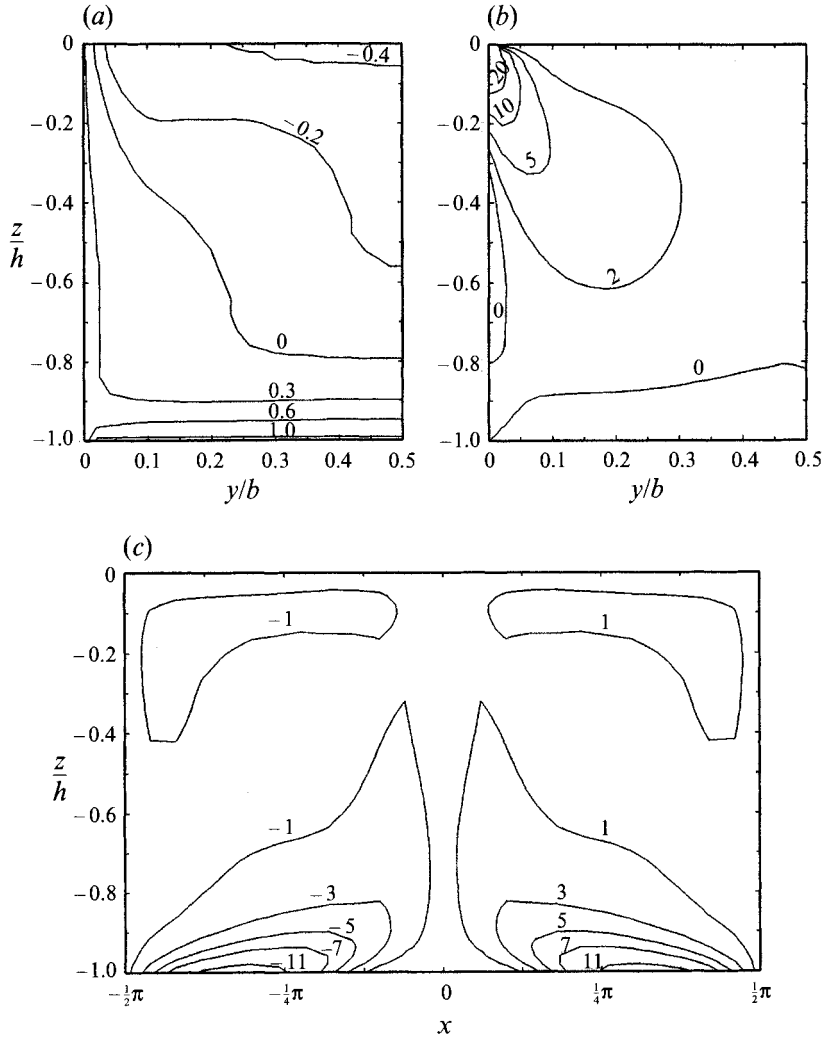

FIGURE 13. As figure 11 but for $\delta = 0.08$.

(ii) The mass transport velocity at the kth time level is calculated from (47) and (48). The vorticity boundary conditions (38) and (39) along the bottom and the sidewall are computed using the current velocity values inside the domain. The first-order derivatives in the boundary conditions are approximated by a second-order finite-difference formula.

(iii) The vorticity transport equation (44) is solved for the vorticity at the new time level, $k+1$, subject to the boundary conditions (34), (35), (36), (37), (38) and (39).

(iv) Steps (i)–(iii) are repeated to obtain the numerical solutions at advanced time levels. Steady-state solutions are reached when the following condition is satisfied:

$$\max_n \frac{|\boldsymbol{\Omega}_n^{k+1} - \boldsymbol{\Omega}_n^k|}{|\boldsymbol{\Omega}_n^{k+1}|} \leqslant 10^{-5}. \tag{49}$$

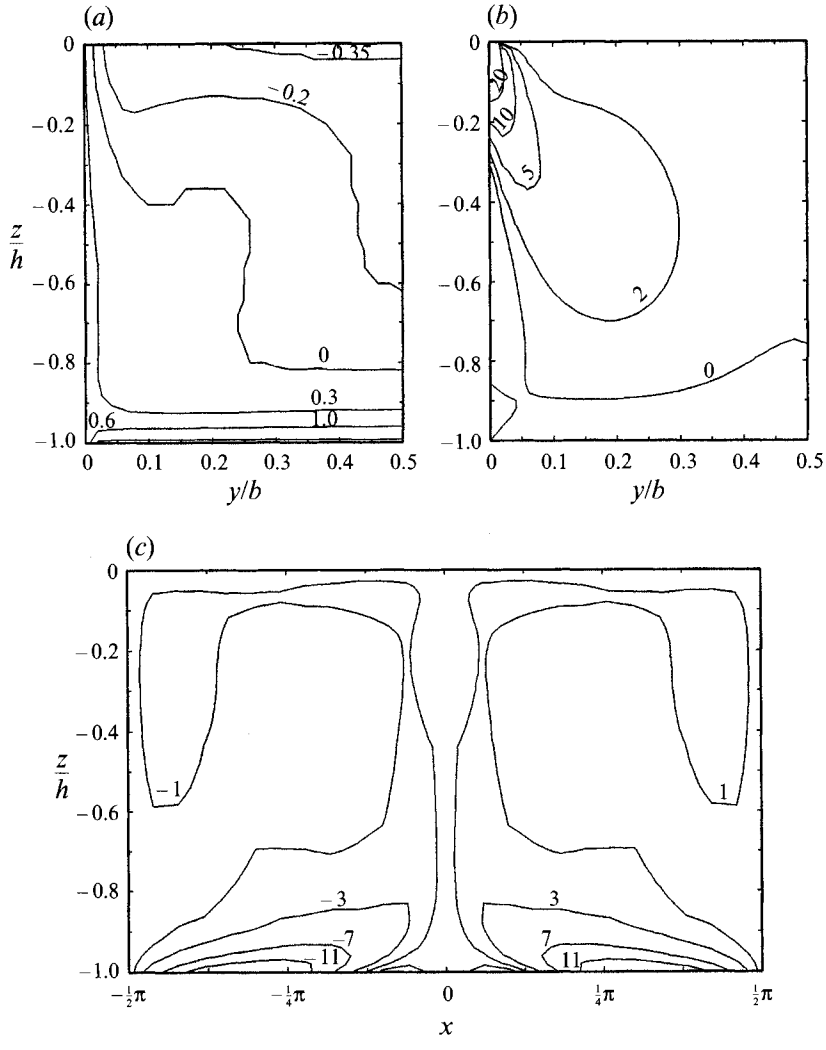

FIGURE 14. As figure 11 but for $\delta = 0.06$.

6. Results and discussion

In this section we present numerical results for the mass transport velocity pattern under partially reflected waves in a long wave tank with a rectangular cross-section. The effects of sidewalls, wave parameter δ and geometric ratio, b/h, on the three-dimensional mass transport pattern are investigated. Note that the reflection coefficient R is a complex-valued constant, i.e. $R = |R|e^{i\theta}$. However, the only impact of the phase, θ, on the mass transport is to shift the flow pattern by $\frac{1}{2}\theta$, i.e. $x \to x - \frac{1}{2}\theta$. This could be seen from the governing equations in §2 and the boundary conditions in §3. Hence, in the following discussions, R will be taken as a real constant, i.e. $\theta = 0$.

6.1. *Comparison between current results and existing solutions*

To verify the present numerical scheme we first obtain numerical solutions for the mass transport velocity in a progressive wave train ($R = 0$) in a channel with a square cross-section ($b = h = 1$). For this example the viscous effects are assumed to be dominant, $\delta = 5 \times 10^5$. Analytical solutions based on the conduction solution approach

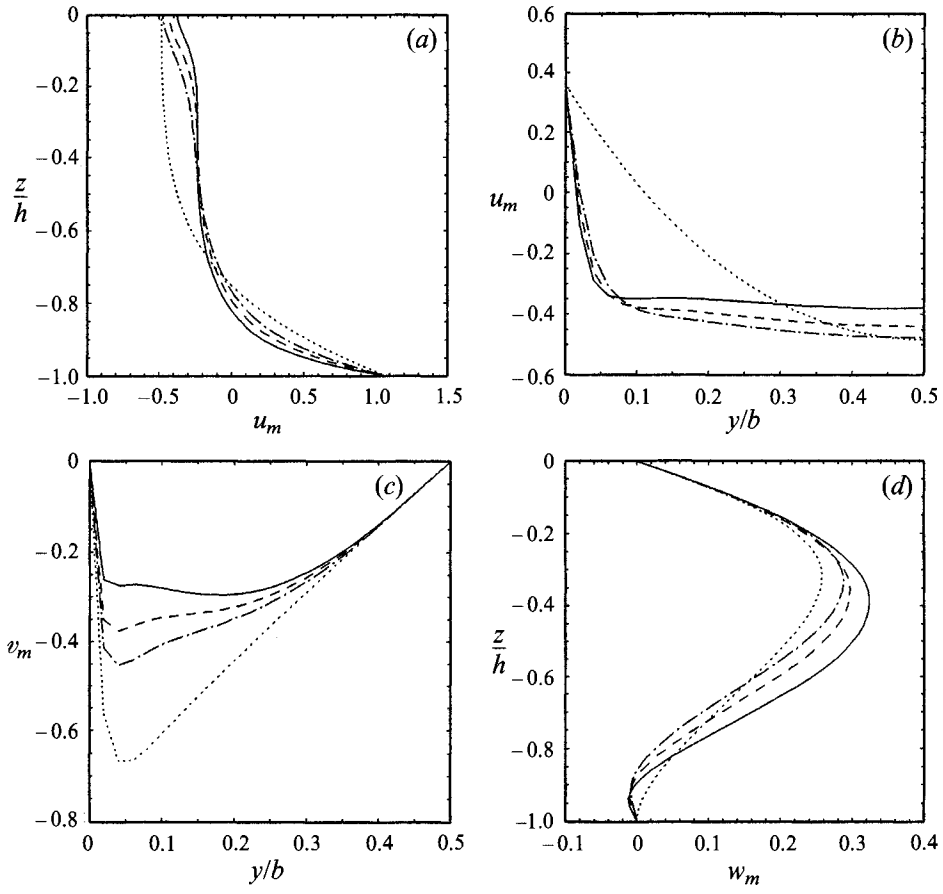

FIGURE 15. Mass transport velocity profiles at $x = -\frac{1}{4}\pi$ for standing waves with different δ: ——, $\delta = 0.06$; – – –, $\delta = 0.08$; —·—, $\delta = 0.1$; - - - - -, $\delta = 100$: (*a*) vertical profiles of u_m on the central plane ($y/b = 0.5$); (*b*) horizontal profiles of u_m on the free surface; (*c*) horizontal profiles of v_m on the free surface; (*d*) vertical profiles of w_m on the central plane ($y/b = 0.5$).

are available (Mei *et al.* 1972). The agreement between the analytical and numerical solutions is excellent. In figure 1 the streamwise mass transport velocity u_m on the central plane, $y/b = 0.5$, is shown. The details of the circulation pattern for this case have been presented in Mei *et al.* (1972) and will not be repeated here. In the same figure the streamwise mass transport velocity for $\delta = 0.1$ is also plotted for comparison. The magnitude of the mass transport velocity on the central plane is reduced significantly when convection becomes important, i.e. small δ-values. The effects of δ on the three-dimensional flow patterns are discussed in §6.3.

The second example for the purpose of verification concerns two-dimensional partially reflected waves, i.e. the sidewall effects are ignored. In the numerical computations the sidewall boundary conditions are altered: the spanwise gradients of all physical quantities are required to vanish, i.e. $\partial/\partial y \equiv 0$. The cross-section of the channel remains a square, $b/h = 1.0$, and the wave parameters δ is chosen to be 0.1. The streamwise mass transport velocity on the central plane at $x = \frac{1}{4}\pi$ for the reflection coefficient $R = 0.5$ and 1.0 is compared with the numerical solutions by Iskandarani & Liu (1991) in figure 2. The numerical scheme used by Iskandarani & Liu (1991), which is limited to two-dimensional problems, is completely different from the present

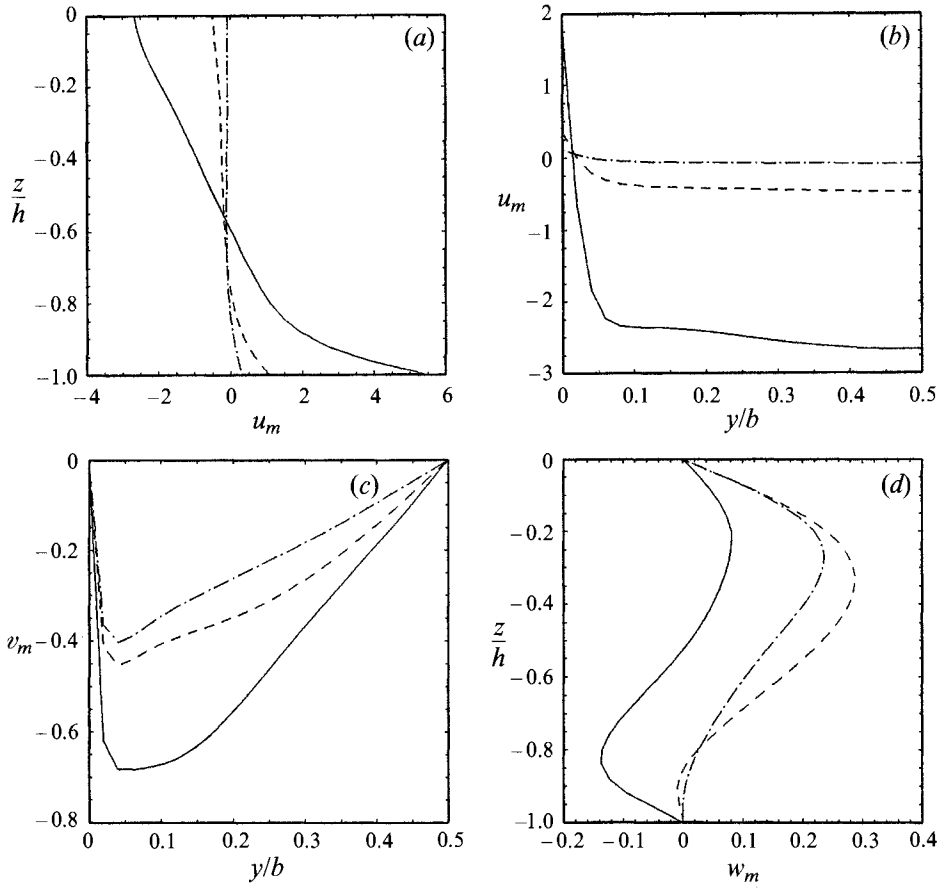

FIGURE 16. Mass transport velocity profiles at $x = -\frac{1}{4}\pi$ for standing waves with different water depth h ($b = 1.0$): ——, $h/b = 0.5$; – – –, $h/b = 1.0$; —·—, $h/b = 1.5$: (*a*) vertical profiles of u_m on the central plane ($y/b = 0.5$); (*b*) horizontal profiles of u_m on the free surface; (*c*) horizontal profiles of v_m on the free surface; (*d*) vertical profiles of w_m on the central plane ($y/b = 0.5$).

approach. However, the agreement between these two sets of numerical results is excellent. In the same figure numerical results for the three-dimensional problems where sidewalls are considered are also plotted for comparison. For the case $R = 0.5$ the mass transport velocity is slower on and near the free surface, and the velocity is more uniform in the mid-depth section.

6.2. *Comparison between current results and experimental data*

Mei *et al.* (1972) reported a series of laboratory experiments measuring mass transport velocity under progressive waves ($R = 0$) in a wave tank. Using a dye tracing technique Mei *et al.* measured mass transport velocity not only on the central plane but also on a vertical plane near the sidewall. In their experiments the wavetank was 76 cm wide and water depth was kept 13 cm deep. Two sets of experimental data are compared to the present theory. The first set is for relatively deep water, $kh = 2.59$, while the second set is for $kh = 1.02$. In figure 3 the experimental data, Longuest-Higgins' (1953) two-dimensional solutions and the present results for u_m along the central plane are plotted for $kh = 2.59$; $\delta = 0.059$. The present solutions agree with the experimental data much better than Longuet-Higgins' two-dimensional solutions do. In figure 4 the second set of laboratory data for u_m on the plane 5 cm away from the sidewall (figure 4*a*) and on

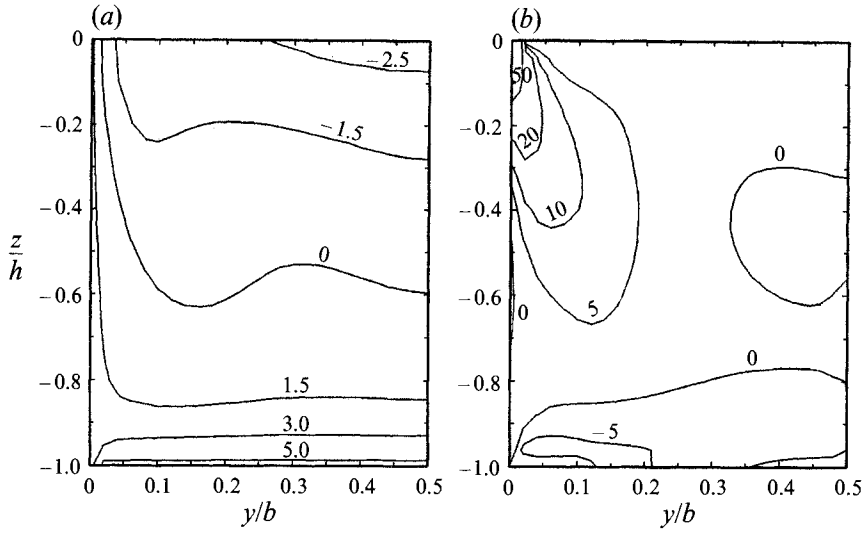

FIGURE 17. Contour lines of u_m, ω^x at $x = -\frac{1}{4}\pi$ for the standing wave with $\delta = 0.1$, $h/b = 1.5$, $b = 1$: (*a*) streamwise mass transport velocity u_m; (*b*) streamwise vorticity ω^x.

the central plane (figure 4*b*) are shown. For this data set $kh = 1.02$ and $\delta = 0.034$. The scattering of the experimental data is partially caused by the unsteadiness of the mass transport velocity; experimental data with different symbols were taken at different times. Despite the data scatter it is clear that the maximum backwards velocity is weaker and closer to the free surface on the plane near the sidewall. The present numerical solutions are produced for this case and are plotted. For the purpose of comparison Longuet-Higgins' two-dimensional solutions, i.e. ignoring the sidewall effects, are also shown. The present results seem to agree with the experimental data better than Longuet-Higgins' two-dimensional solutions do.

In the following section, new numerical results for mass transport under a partially reflected wave train propagating in a rectangular channel are present.

6.3. *Mass transport in a channel with a square cross-section*

In this section numerical results are obtained for a channel with a square cross-section, $b = h = 1$. Numerical computations were performed for different amplitudes (i.e. δ-values) and reflection coefficients (R-values).

In figure 5 the spanwise profiles of the streamwise mass transport velocity, u_m, are plotted. These velocity profiles are for $x = -\frac{1}{4}\pi$ and $z/h = -0.8$, -0.5, -0.2 and 0 respectively. These results are obtained for $\delta = 0.1$ and $R = 0$, 0.5, and 1.0 respectively. Note that u_m varies periodically in the x-direction for a partially reflected wave but becomes uniform for a progressive wave ($R = 0$). For the standing wave ($R = 1.0$) the cross-section $x = -\frac{1}{4}\pi$ is the midpoint between a node and an anti-node. From figure 5 we observe that the mass transport velocity, u_m, along the sidewall ($y/b = 0$) is always positive. There is a small region, $0 < y/b < 0.1$, in which the mass transport velocity changes drastically. The mass transport velocity becomes more or less uniform in the y-direction outside this region. This suggests that there is a boundary layer formed outside of the Stokes boundary layer because of the small δ-value.

In figure 6 the vertical profiles of the mass transport velocity for the same set of parameters used in figure 5 are shown. These profiles are plotted for different planes parallel to the sidewall, $y/b = 0.1$, 0.3, and 0.5. There are slight differences between the

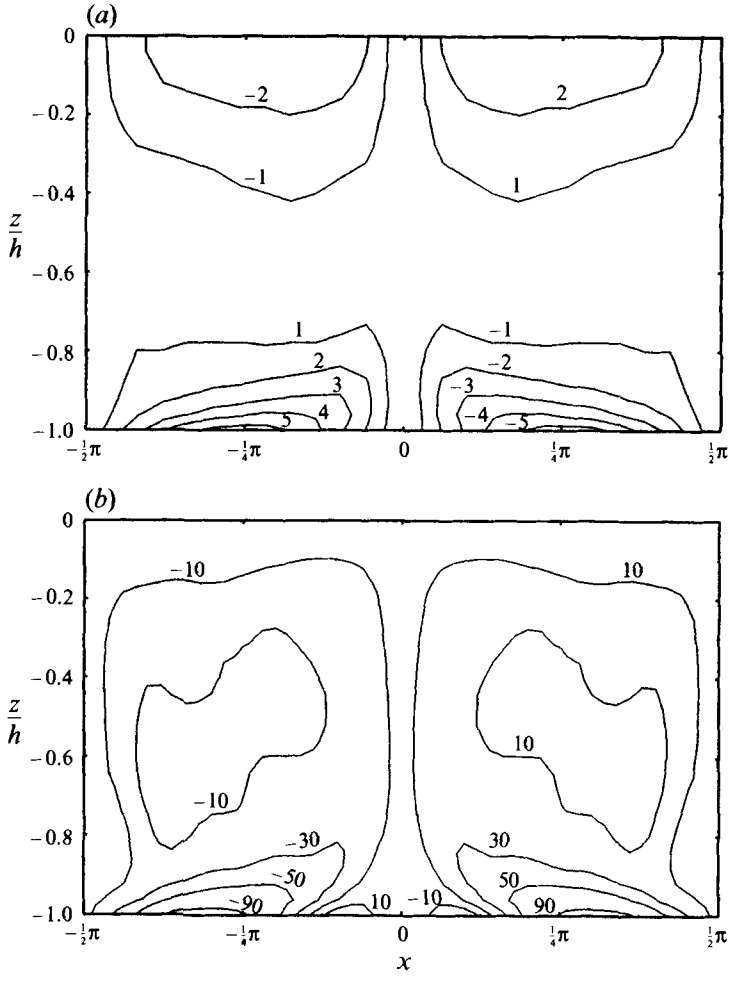

FIGURE 18. Contour lines of u_m, ω^y on the central plane ($y/b = 0.5$) for the standing wave with $\delta = 0.1$, $h/b = 1.5$, $b = 1$: (*a*) streamwise mass transport velocity u_m; (*b*) spanwise vorticity ω^y.

profiles at $y/b = 0.3$ and 0.5. However, the velocity is weaker and the profile is considerably different near the sidewall ($y/b = 0.1$). The appearance of boundary layers near the free surface and the bottom for $R = 0$ and 0.5 is quite clear. However, for the standing wave ($R = 1.0$) the boundary layer near the free surface diminishes. For the progressive wave the mass transport velocity profile on the central plane is also shown in figure 1. As shown in figure 1 when δ is increased the diffusion becomes important and the boundary-layer structure disappears even for the progressive case. For comparison the two-dimensional results (without the sidewall effects) are also shown in figure 6. The two-dimensional results are again without the boundary-layer structure and are remarkably different from those including the sidewall effects. Because u_m varies periodically in the x-direction for a partially reflected wave, the contour lines of u_m are plotted on the central plane ($y/b = 0.5$) in figure 7 and on the free surface ($z/h = 0$) in figure 8. The mass transport velocity contours evolve from parallel horizontal lines for the progressive wave ($R = 0$) to an antisymmetric cell structure for the standing wave ($R = 1.0$). Large velocity gradients are clearly visible near the bottom and the sidewall, indicating the existence of boundary layers.

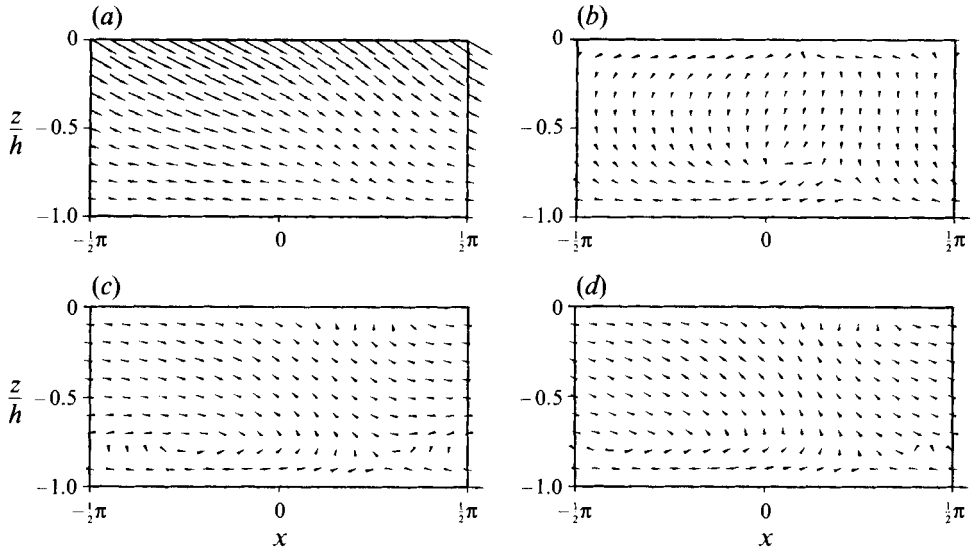

FIGURE 19. Projection of mass transport velocity under a partially reflected wave ($R = 0.5$) on planes parallel to the sidewall with $\delta = 0.1$, $h/b = 1$, $b = 1$: (*a*) $y/b = 0$; (*b*) $y/b = 0.1$; (*c*) $y/b = 0.3$; (*d*) $y/b = 0.5$.

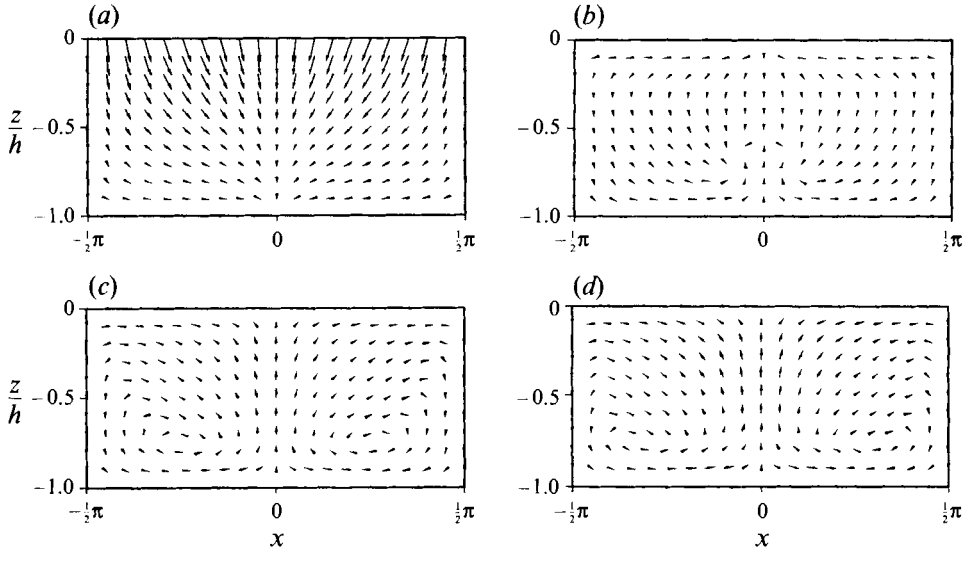

FIGURE 20. As figure 19 but under a standing wave ($R = 1.0$).

The vertical profiles of the spanwise mass transport velocity v_m on the plane $x = -\frac{1}{4}\pi$ are shown in figure 9. For all cases ($R = 0$, 0.5 and 1.0) v_m is negative in the upper region (near the free surface), and positive in the low region (near the bottom). Therefore fluid particles move towards the sidewalls in the upper region and move away from the sidewalls towards the central plane in the lower region. The vertical component of the mass transport velocity is shown in figure 10 for different reflection coefficients. Near the sidewall the mass transport moves downwards on all elevations and the mass transport velocity component becomes positive near the middle of the tank. So a fluid particle which starts initially near the central plane and just beneath

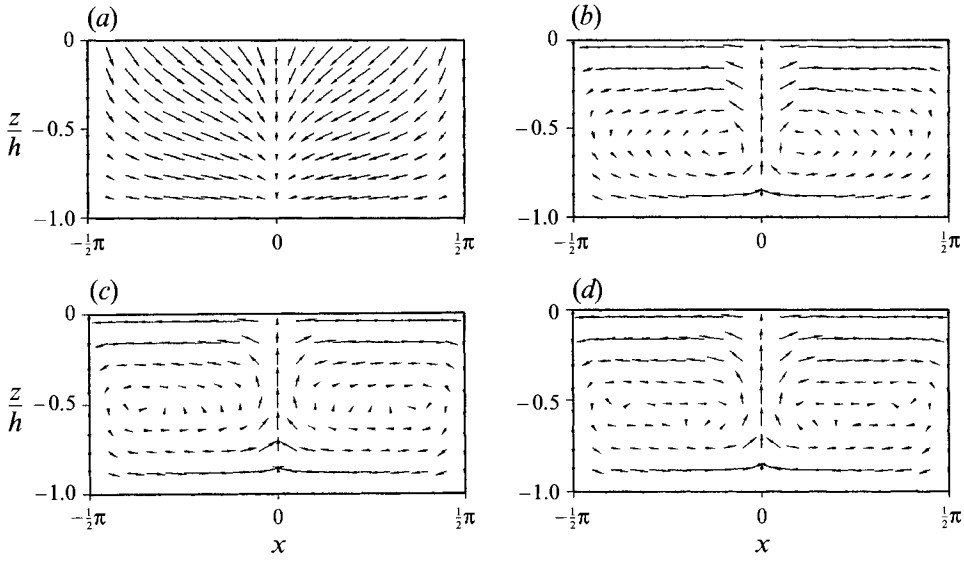

FIGURE 21. As figure 20 but for $h/b = 0.5$.

the free surface will move towards the sidewall and rise slightly. As the particle moves close to the sidewall, it starts to move downwards. When the particle drops to the mid-depth level, it begins to move away from the sidewall. Eventually it will rise towards the free surface again near the central plane. The circulation pattern will be repeated. Of course one should keep in mind that the particle is also transported by the streamwise mass transport velocity, u_m. Therefore the particle will not stay in the same vertical plane perpendicular to the x-direction. A very complex three-dimensional drift pattern exists in the channel caused by the sidewall effects.

The effects of δ (nonlinearity) on the mass transport velocity pattern are shown for the standing waves only. The contour lines of the streamwise mass transport u_m and the streamwise vorticity ω^x at $x = -\frac{1}{4}\pi$ (midpoint between nodal and anti-nodal point) as well as the spanwise vorticity ω^y on the central plane ($y/b = 0.5$) are plotted in figures 11, 12, 13, and 14 for $\delta = 100$, 0.1, 0.08, and 0.06, respectively. The vertical profiles of the streamwise velocity u_m and the vertical velocity w_m on the central plane, and the horizontal profiles of u_m and the spanwise velocity v_m on the free surface ($z/h = 0$) are shown in figure 15. The dependence of mass transport on the δ-values is apparent. For a large δ-value (figure 11) diffusion dominates and vorticities are diffused into the interior region. As the δ-value decreases, convection becomes more important and vorticities are confined in the boundary layers adjacent to the bottom and the sidewall (figures 13 and 14).

6.4. *Mass transport in channels with different geometric ratios* (h/b)

To investigate the effects of the tank geometry, we present here numerical results for standing waves in rectangular channels with different geometric ratios, i.e. h/b-values. The vertical profiles of the streamwise velocity u_m and the vertical velocity w_m on the central plane ($y/b = 0.5$), and the horizontal profiles of u_m and the spanwise velocity v_m on the free surface ($z/h = 0$) are shown in figure 16 for $h/b = 0.5$, 1.0, 1.5. When h/b is small (the tank is relatively wide and the depth is relatively shallow), the horizontal velocity components (u_m, v_m) become large, while the vertical component w_m is small. The boundary-layer structure near the sidewalls is also more prominent. For a wider

tank, ($h/b = 0.5$) the vertical profile of the streamwise mass transport velocity u_m on the central plane, at $x = -\frac{1}{4}\pi$, resembles that of the two-dimensional case (without the sidewalls shown in figure 6(*c*). Away from the sidewalls, the bottom boundary has more important effects on the mass transport in the core region. The contour lines of the streamwise mass transport u_m and the streamwise vorticity ω^x at $x = -\frac{1}{4}\pi$ for $h/b = 0.5$ are shown in figure 17. Figure 18 shows the contour lines of the streamwise velocity u_m and the spanwise vorticity ω^y on the central plane for the case with the same parameters as in figure 17. The distributions of the mass transport velocity outside the sidewall boundary layer are more uniform for the channel with smaller h/b values. Vorticity is mostly confined to the neighbourhood of the sidewalls and the bottom.

Figures 19, 20 and 21 present the projection of mass transport velocity on the planes parallel to the sidewalls (y/b = constant). In figure 19 the water depth is $h = 1.0$, and the reflection coefficient R is 0.5. Figures 20 and 21 are for standing waves ($R = 1.0$). In figure 21 the depth is shallower, $h = 0.5$, while $h = 1.0$ in figure 20. In all these cases δ is 0.1 and the width b is 1.0. The vectors in these figures are the two-dimensional mass velocity vectors formed by (u_m, w_m) on the y-plane.

7. Concluding remarks

A vorticity-vector potential scheme with a Fourier spectral method has been developed to study the three-dimensional mass transport induced by partially reflected waves in a rectangular channel. Attentions have been focused on three issues: (i) the effects of the sidewalls on the mass transport pattern; (ii) the effects of the wave amplitude (δ-values) and (iii) the effects of the tank geometric ratio (h/b-values). Numerical results show that the presence of the sidewalls generates complicated three-dimensional mass transport velocity patterns. Even for a relatively wide channel, e.g. $b/h = 6$, the mass transport velocity, u_m, under a progressive wave is still influenced by the sidewall effects (see figure 3 and 4). Therefore in performing laboratory experiments one must be precise about the location of the sampling points. Moreover, the mass transport velocity has a spanwise component which moves particles from the central region of the tank towards the sidewall near the free surface and from the sidewall region towards the central plane in the lower half of the depth. This flow pattern is not very sensitive to reflection coefficient. The wave amplitude (or δ-parameter) also plays an important role in determining the mass transport velocity pattern. When δ is small or the amplitude is large convection is important and diffusion is significant only within a small region (double boundary layer) adjacent to the Stokes layers.

High-quality experimental data are rare. The present theoretical results have been compared with Mei *et al.*'s (1972) data; the agreement is reasonable. With new sensors such as laser Doppler velocimetry detailed measurements of three-dimensional mass transport should be obtained.

This research was supported by a grant from the National Science Foundation (CTS–8902407). Computer facilities and funds were provided by the Cornell National Super-computer Facility (CNSF).

REFERENCES

Bijker, E. W., Kalwijk, J. P. Th. & Pieters, T. 1974 Mass transport in gravity waves on a slopping bottom. *Proc. Fourteenth Coastal Engrg. Conf.*, pp. 447–465. ASCE.

Dore, B. D. 1976 Double boundary layer in standing waves. *Pure Appl. Geophys.* **114**, 629–637.

HADDON, E. W. & RILEY, N. 1983 A note on the mean circulation in standing waves. *Wave Motions* **5**, 43–48.

HARA, T. & MEI, C. C. 1987 Bragg scattering of surface waves by periodic bars: theory and experiment. *J. Fluid Mech.* **178**, 221–241.

HIRASAKI, G. J. & HELLUMS, J. D. 1968 A general formulation of the boundary conditions on the vector potential in three-dimensional hydrodynamics. *Q. Appl. Maths* **26**, 331–342.

HIRASAKI, G. J. & HELLUMS, J. D. 1970 Boundary conditions on the vector and scalar potentials in viscous three-dimensional hydrodynamics. *Q. Appl. Maths* **28**, 293–296.

ISKANDARANI, M. & LIU, P. L.-F. 1991 Mass transport in two-dimensional water waves. *J. Fluid Mech.* **231**, 395–415.

ISKANDARANI, M. & LIU, P. L.-F. 1993 Mass transport in a wave tank. *J. Waterway, Port, Coastal, Ocean Engng* **119**, 88–104.

LIU, P. L.-F. 1977 Mass transport in the free surface boundary layer. *Coastal Engng* **1**, 207–219.

LONGUET-HIGGINS, M. S. 1953 Mass transport in water waves. *Phil. Trans. R. Soc. Lond.* A **245**, 535–581.

MEI, C. C. 1989 *The Applied Dynamics of Ocean Surface Waves*. Advanced Series on Ocean Engineering, Vol. 1. World Scientific.

MEI, C. C. & LIU, P. L.-F. 1973 The damping of surface gravity waves in a bounded liquid. *J. Fluid Mech.* **59**, 239–256.

MEI, C. C., LIU, P. L.-F. & CARTER, T. G. 1972 Mass transport in water waves. *Ralph M. Parson Laboratory for Water Resources and Hydrodynamics. Rep.* 146. MIT, Cambridge, Massachusetts.

RILEY, N. 1965 Oscillating viscous flows. *Mathematika* **12**, 161–175.

RUSSELL, R. C. H. & OSORIO, J. C. D. 1958 An experimental investigation of drift profiles in a closed channel. *Proc. VI Conf. on Coastal Engng*, pp. 171–193. ASCE.